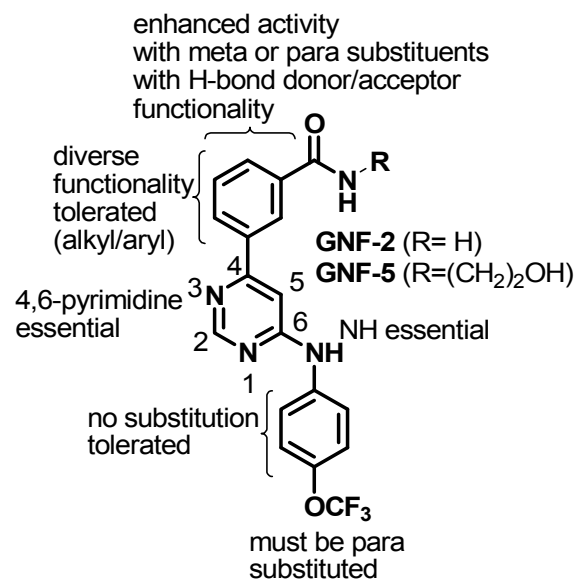


**Figure S1**

**a**



**b**

Bcr-Abl Mutation	G250E	E255V	T315I	F317L	M351T
IC50 ( $\mu$ M)	4.52	0.38	> 5	> 10	0.93

**Figure S2**

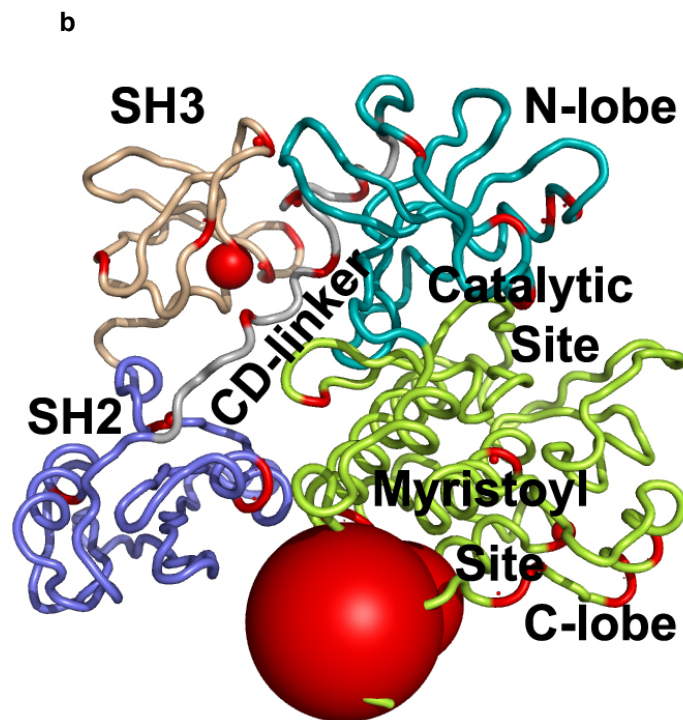
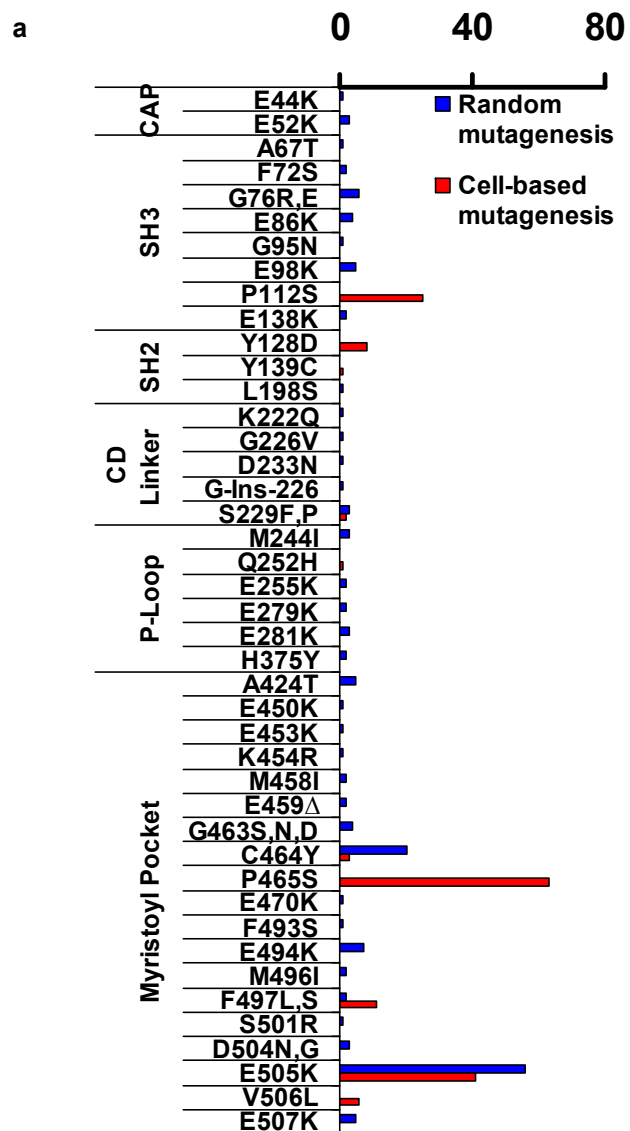
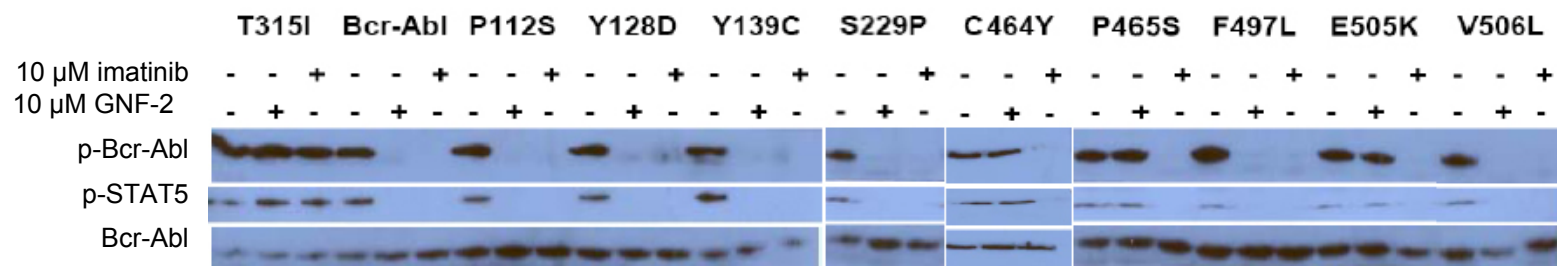
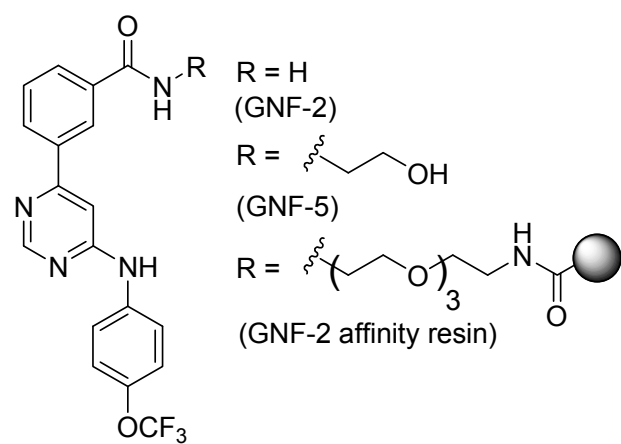


**Figure S3**

**a**



**b**



**c**

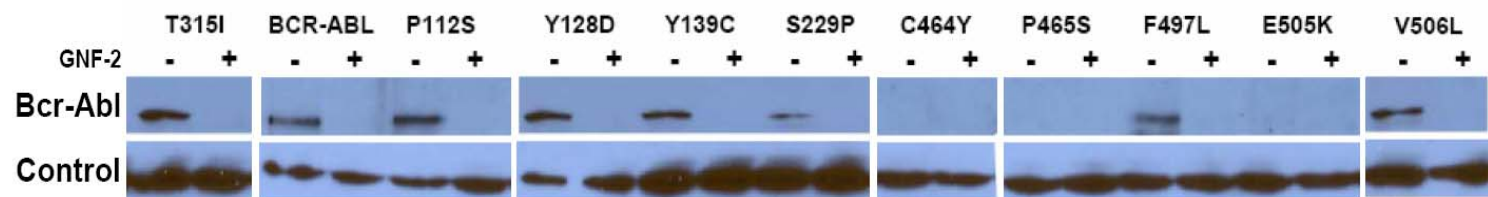
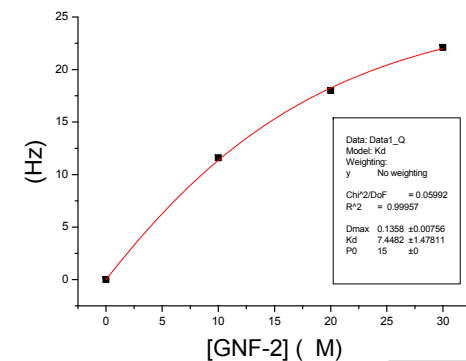
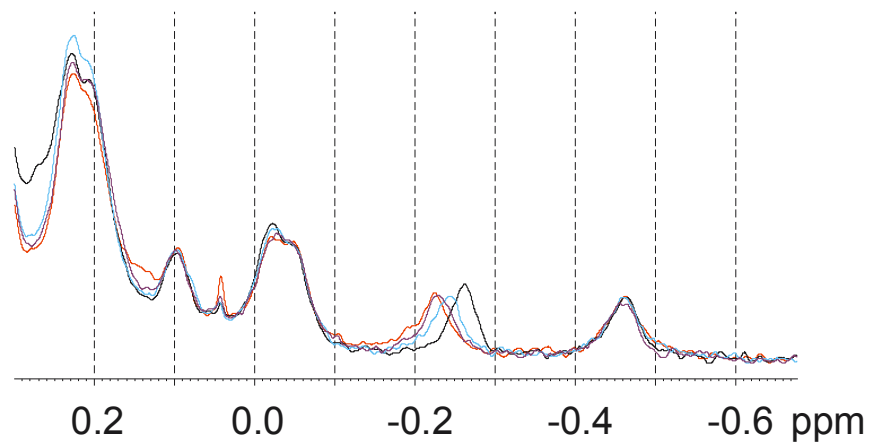
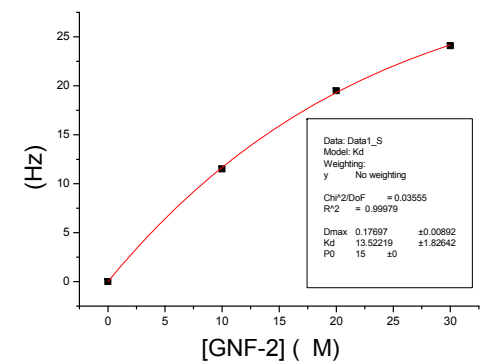
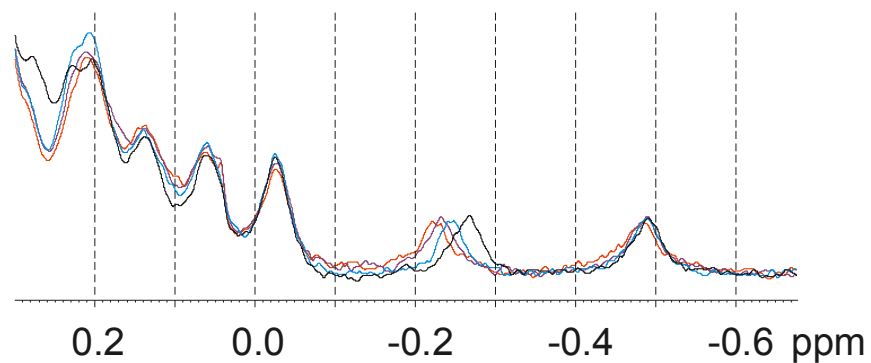


**Figure S4**

**a**  
wt Abl(229-500)



**b**  
T315I Abl(229-500)



**c**  
wt Abl(229-515)

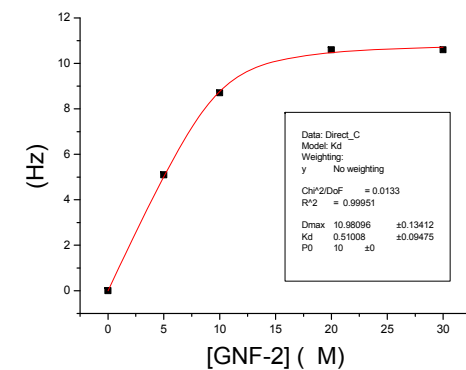
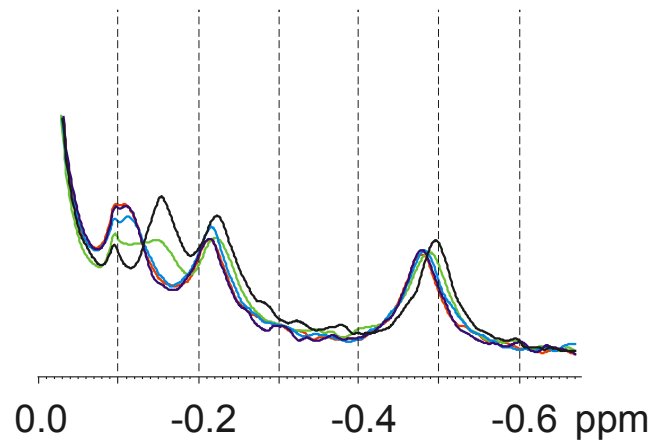
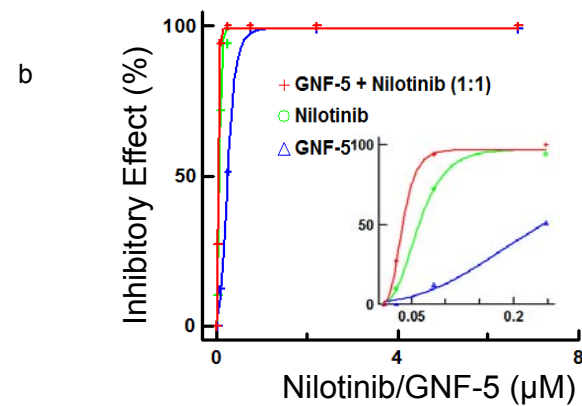
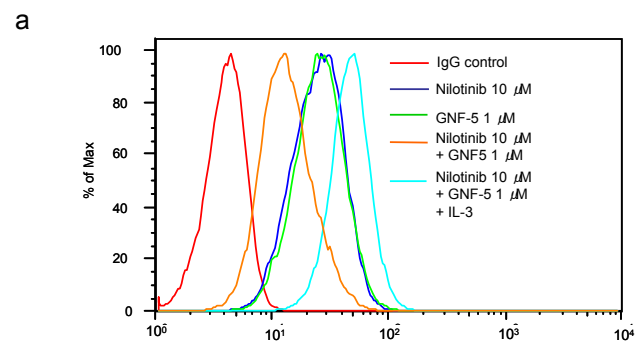


**Figure S5**



c

GNF-5 ( $\mu$ M)	10	5.0	2.0	1.0
BCR-ABL T315I	<0.003	0.24 $\pm$ 0.03	0.80 $\pm$ 0.05	3.55 $\pm$ 0.7
BCR-ABL T315I + IL3	>10	>10	>10	>10
BCR-ABL T315I/E505K	2 $\pm$ 0.07	3.75 $\pm$ 0.17	>5	>10
Ba/F3 + IL3	>10	>10	>10	>10

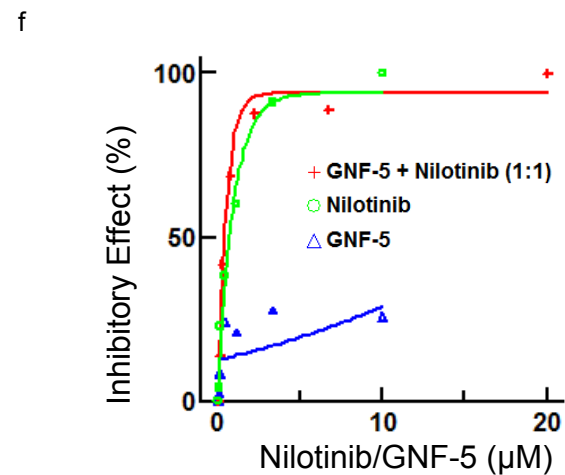
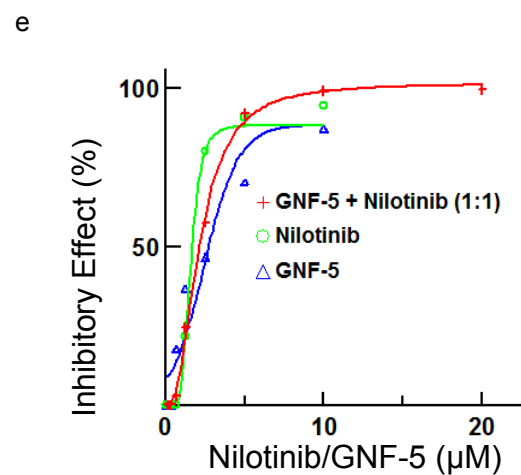
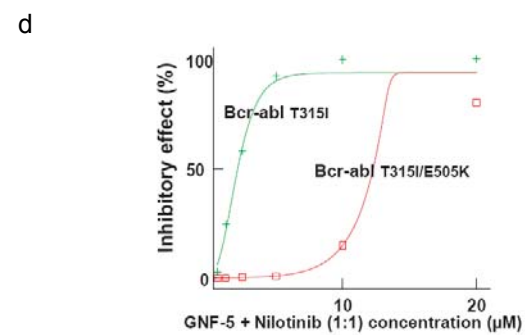
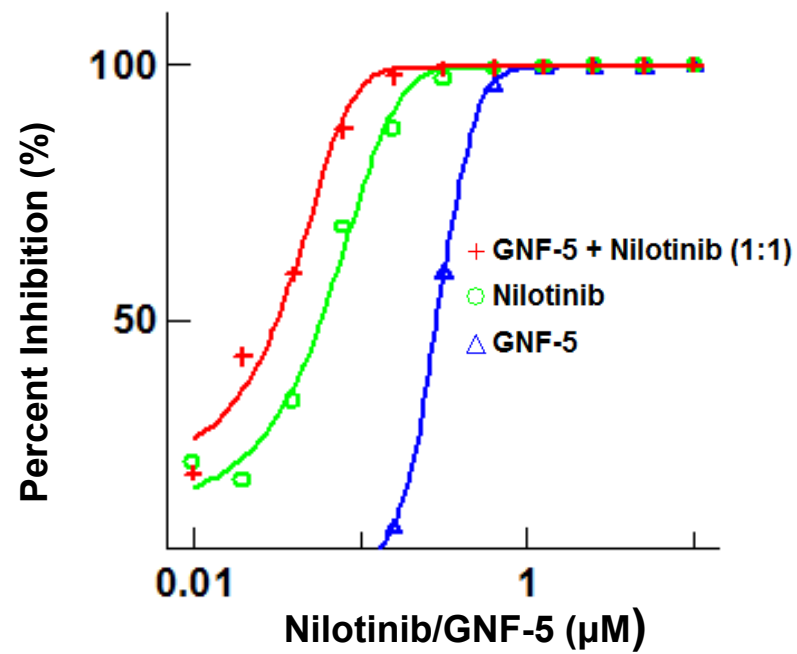
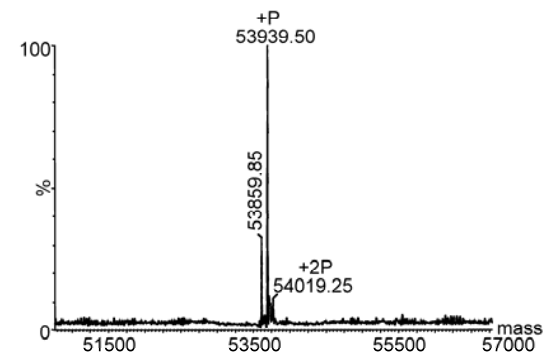
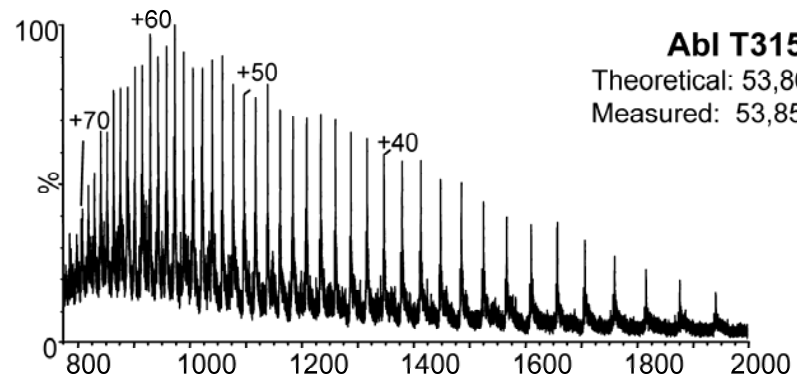
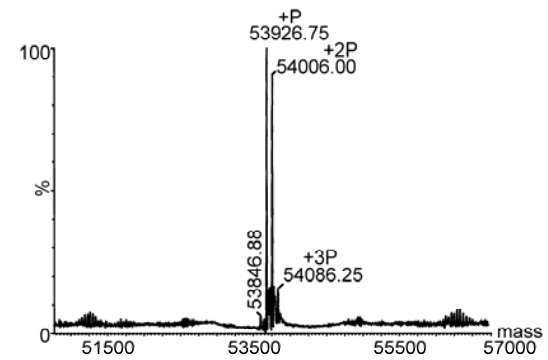
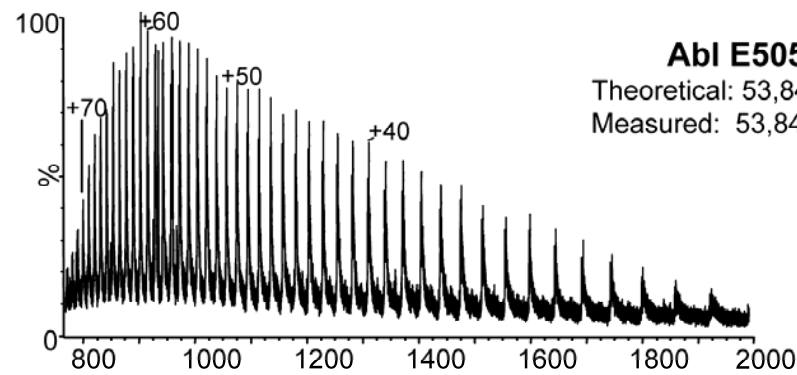
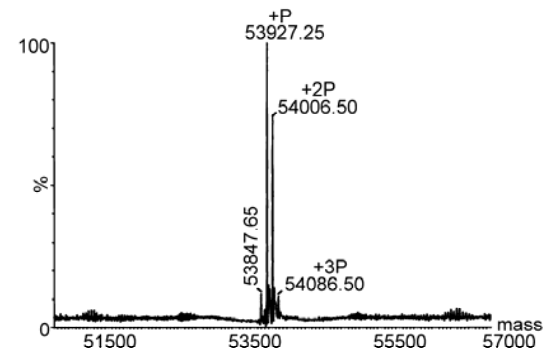
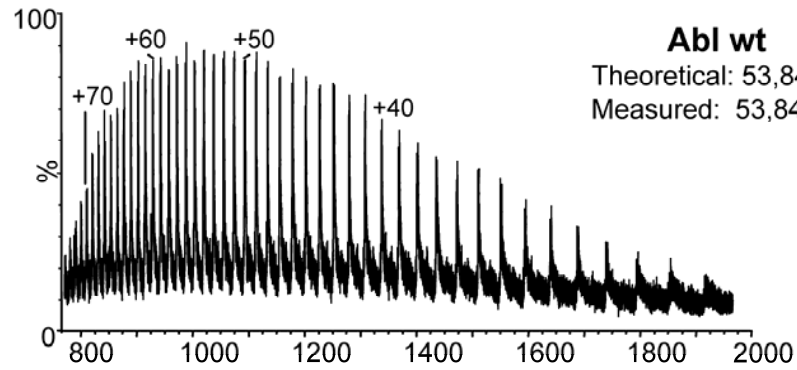


Figure S6



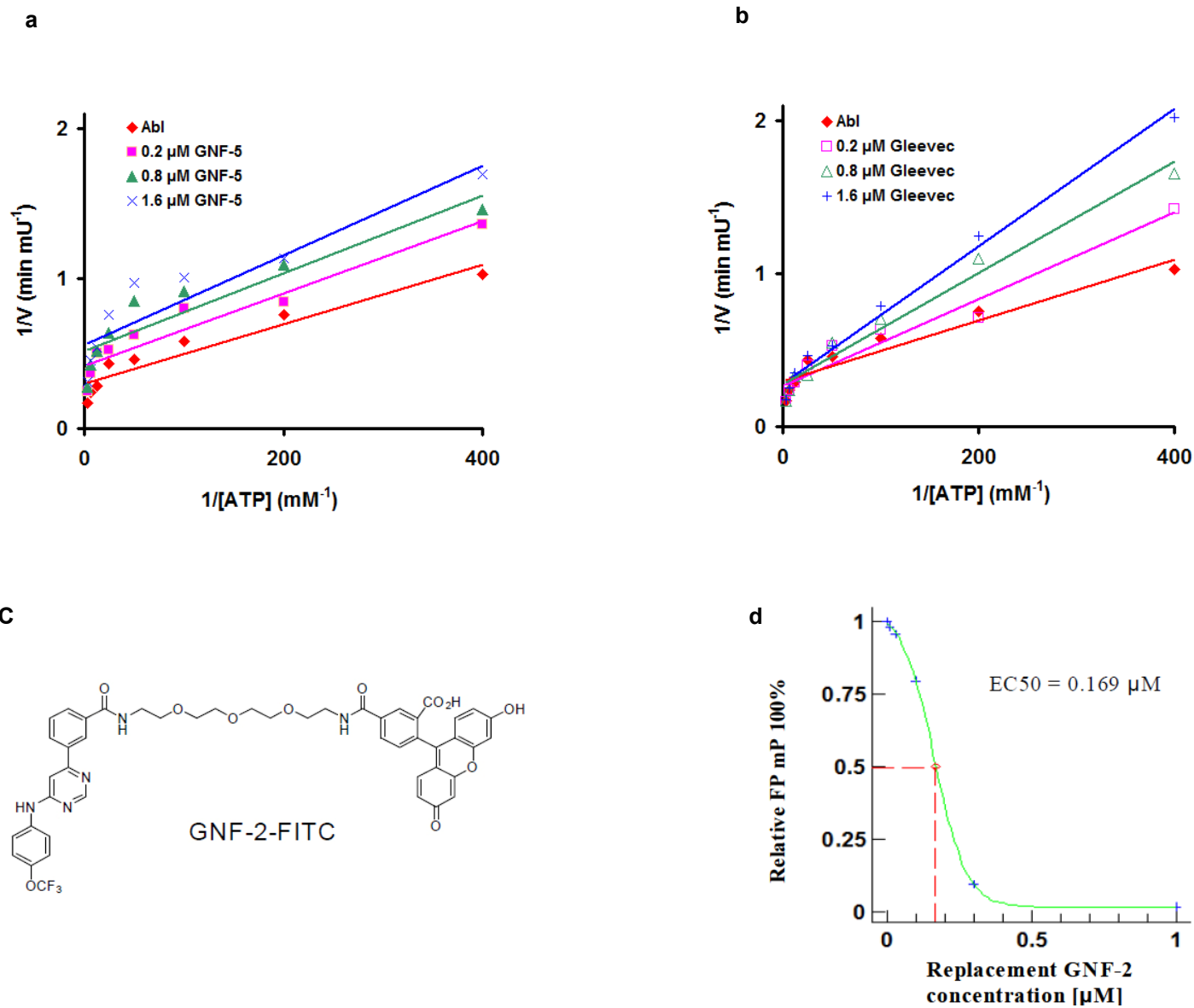
Drug	Combination Index Values at			
	ED50	ED75	ED90	EC50
Nilotinib (Not a combination)	N/A	N/A	N/A	0.036
GNF-5 (Not a combination)	N/A	N/A	N/A	0.376
Nilotinib + GNF-5 (1:1)	0.52003	0.57167	0.63792	0.017

Figure S7



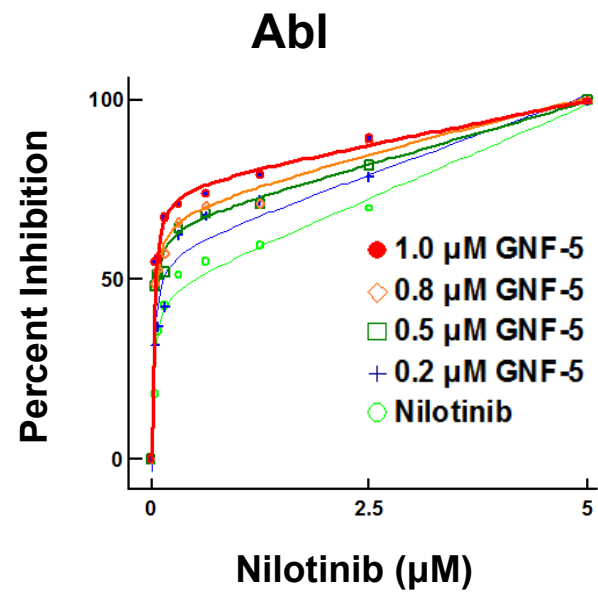
**Figure S8**

mass / charge



**Figure S9**

a



b

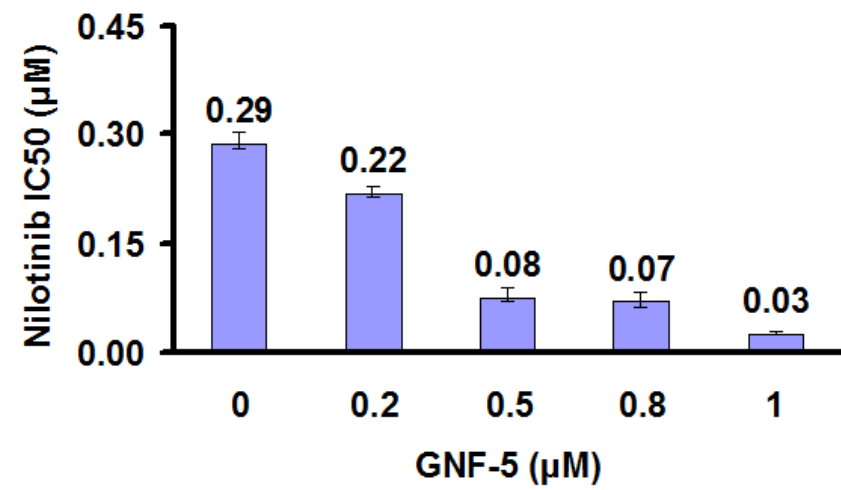
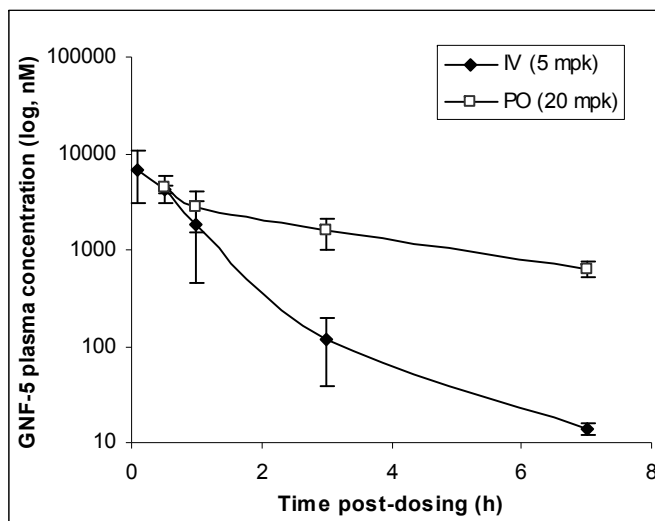
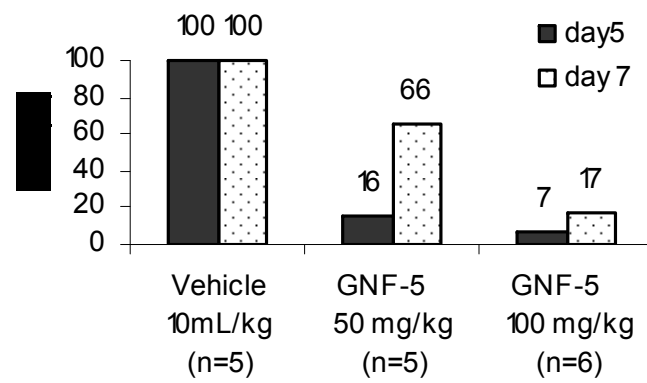


Figure S10

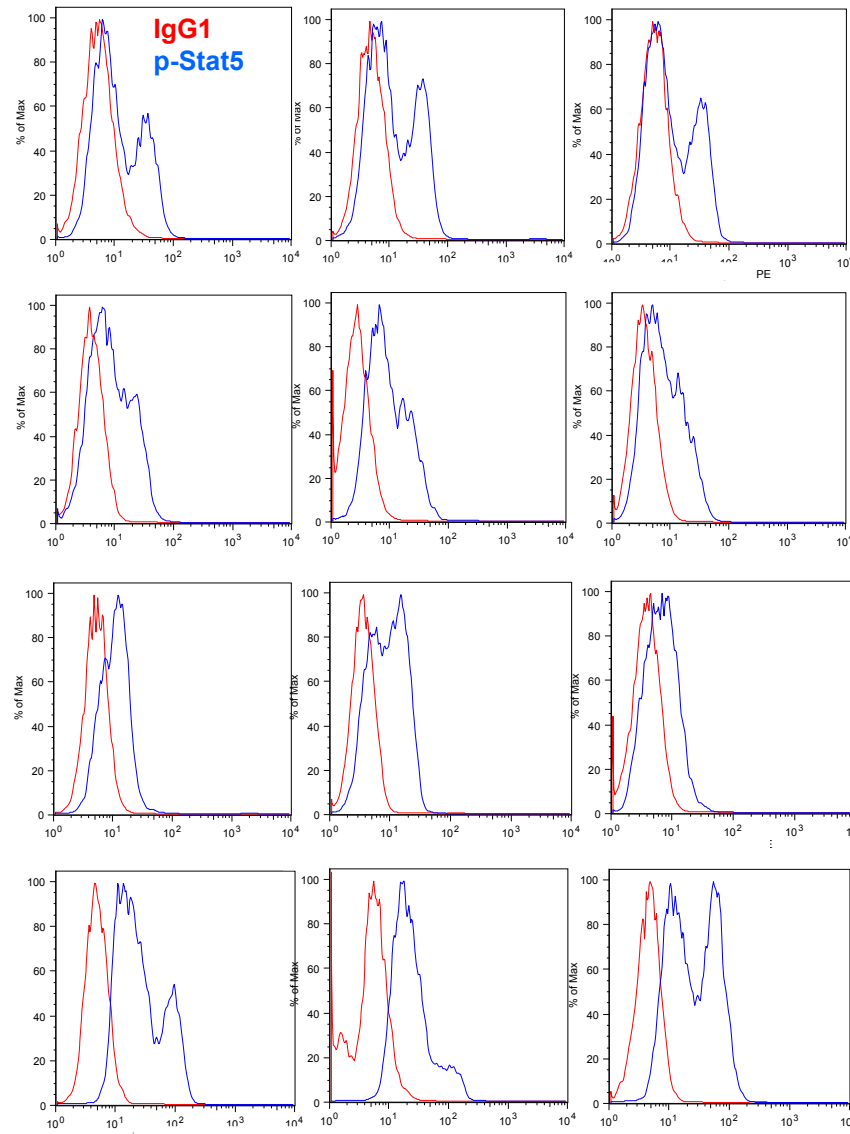
**a****b**

<b>AUC_inf (min*ug/mL)</b>	292.37	±	49.18
<b>AUC_inf (hrs*nM)</b>	11647	±	1959
<b>Cmax (nM)</b>	4386.08	±	1344.67
<b>Tmax (hrs)</b>	0.50	±	0.00
<b>Clast (nM)</b>	636.16	±	121.20
<b>T1/2 (hrs)</b>	2.30	±	0.10
<b>Vss (L/kg)</b>	9.18	±	1.82
<b>F (%)</b>	44.82	±	7.54

**Figure S11**



**Figure S12**



**vehicle n=3**

**GNF-5 100 mg/kg, 3 h; n=3**

**GNF-5 100 mg/kg, 7 h; n=3**

**GNF-5 100 mg/kg, 24 h; n=3**

**Figure S13**

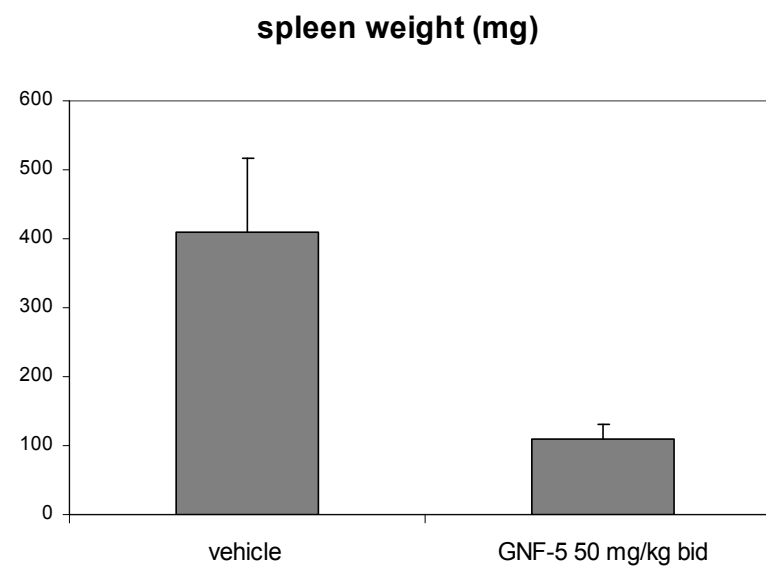
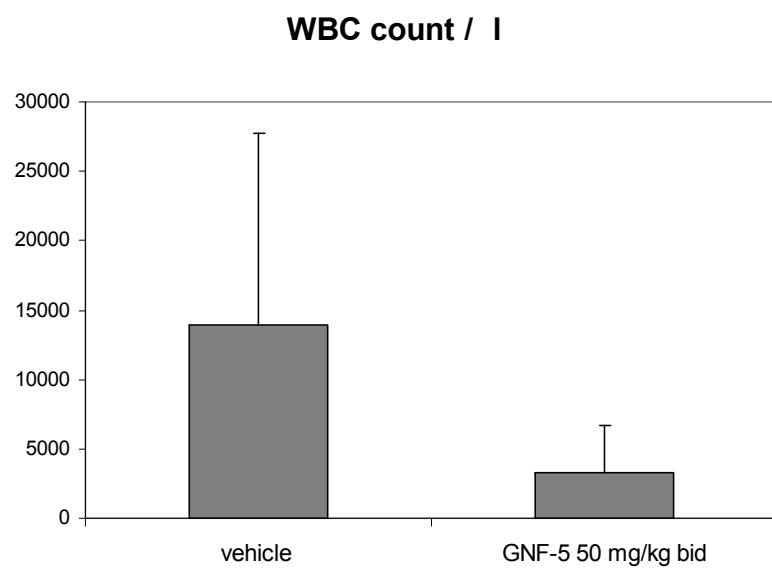


**Figure S14**

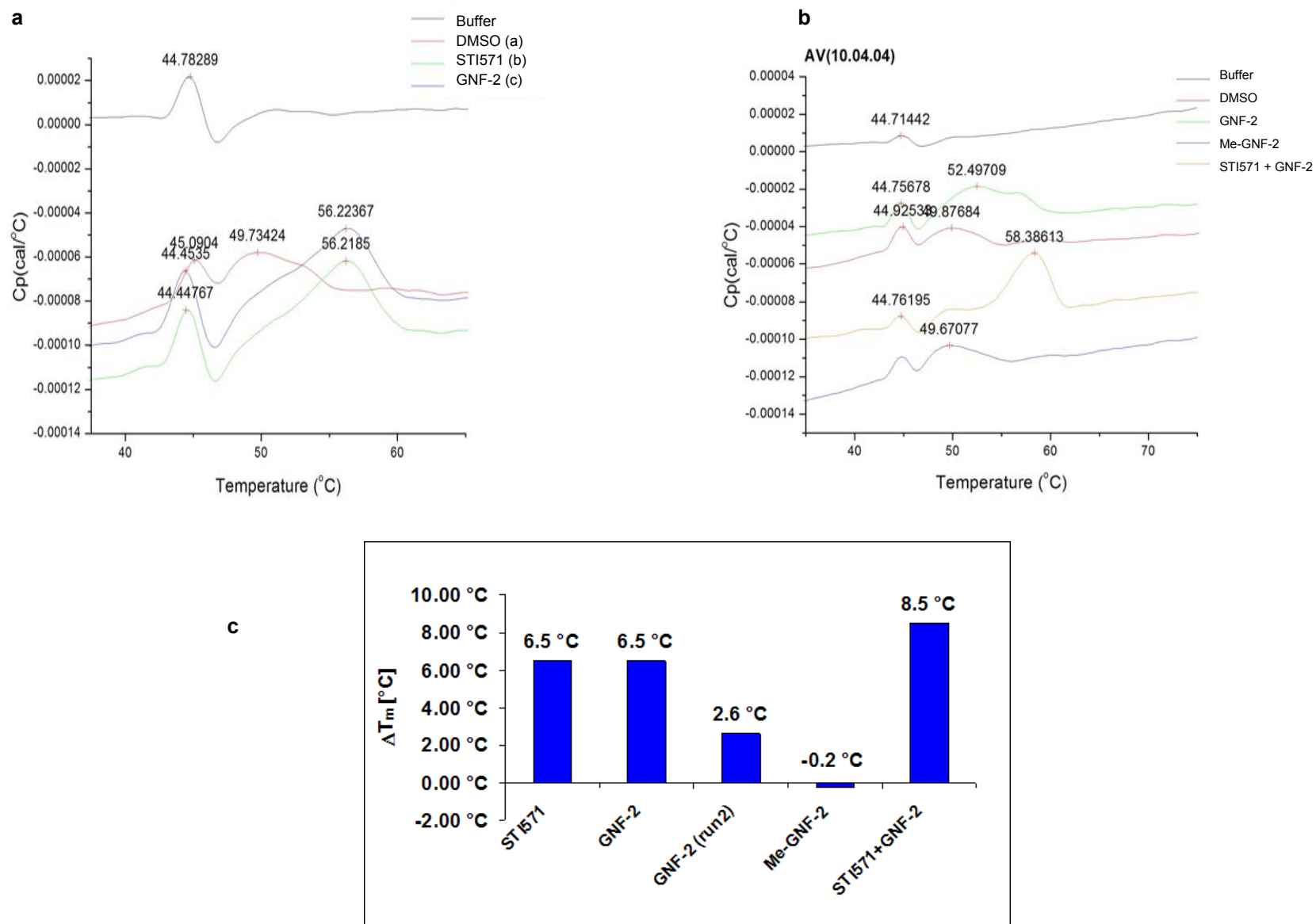


Figure S15

## Supplemental Methods

### Protein preparation for crystallography:

A construct of Abl kinase domain (mouse c-Abl, residues 229-515, Abl 1a numbering) as described by Nagar et al<sup>1</sup> was expressed in Sf9 insect cells with imatinib (16  $\mu$ M final concentration) added to the culture at the time of viral infection. Cells were lysed by sonication in buffer A (50 mM Na-phosphate, 300 mM NaCl, 10% v/v glycerol, 10 mM 2-Mercaptoethanol, pH 8.0) supplemented with a protease inhibitor cocktail (Complete-EDTA free, Roche) and 20  $\mu$ M of imatinib. The lysate was clarified by centrifugation (40,000 X g, 2 h, 4 °C) and subsequent filtration. The filtrate was loaded on Ni-NTA superflow (Qiagen), the resin washed with 15 mM imidazole in buffer A, then with 12.5 mM imidazole in buffer B (20 mM Tris, 100 mM NaCl, 10 % v/v glycerol, pH 8.0 at 4 °C). His-Abl / imatinib was eluted with 125 mM imidazole in buffer B and - after addition of 1 mM EDTA and 2.5 mM DTT - incubated with AcTEV protease (Invitrogen) at 4 °C to remove the His-tag. After 17 h the reaction was diluted to 50 mM NaCl with buffer C (20 mM Tris, 5% v/v glycerol, 2 mM DTT, pH 8.3 at 4 °C) and loaded on a MonoQ HR 10/10 column (GE Healthcare). Abl/imatinib was eluted with a linear gradient from 50 to 300 mM NaCl in buffer C in 25 column volumes. Fractions containing unphosphorylated Abl/imatinib were pooled, concentrated, loaded on a Superdex 75 HiLoad 16/60 column (GE Healthcare) and eluted with buffer D (20 mM Tris, 100 mM NaCl, 1 mM EDTA, 3 mM DTT, pH 7.6 adjusted at 23 °C). The single peak observed, corresponding to monomeric Abl/imatinib complex, was concentrated to 20 mg/ml. Final quality control by LC-MS yielded a mass of 33705.0 Da (expected mass 33704.5 Da for unphosphorylated, reduced GAMDPS- mouse Abl (229-515)).

### Crystallization and data collection:

Crystals were grown as described in Nagar et al<sup>1</sup> using the conditions listed in Table S1. After soaking for 7 days at 4°C in a solution containing 1 mM GNF-2, the crystals were cryo-cooled and stored in liquid nitrogen. Data were collected from a single crystal at beamline PXII of the Swiss Light Source (Table S1). A complete data set was collected using a MARCCD 225 after 360 degrees of rotation with 1 degree rotation ranges for each image. Data were processed inside APRV<sup>2</sup> using XDS<sup>3</sup>.

**Table S1. Crystallization and data collection**

Protein solution	20 mg/ml
Crystallization buffer	0.1M MES pH 5.6, 0.2M MgCl <sub>2</sub> , 18% PEG4000
Wavelength (Å)	1.00160
Space group	P1
Number of molecules in A.U.	2
Unit Cell (Å; degrees)	42.1, 65.3, 66.3; 72.8, 80.2, 84.9
Resolution range (highest shell) (Å)	62.50-1.74 (1.80-1.74)
Rsym (%)	4.5 (38.2)

I/sig(I) (%)	16.5 (3.4)
Completeness (%)	95.3 (86.2)
Multiplicity (%)	3.9 (3.6)
Observed reflections (Unique)	254609 (64929)
Wilson B-factor ( $\text{\AA}^2$ )	31.8

### Structure refinement:

The structure was solved using rigid body refinement and difference Fourier methods with Refmac5<sup>4</sup> and the protein coordinates of PDB entry 1OPJ as a starting model. Refinement proceeded with cycles of model building using the molecular graphics program COOT<sup>5</sup> and maximum likelihood based minimisation using Refmac5. Imatinib and GNF-2 were fitted to clear difference electron density (Figure S2), and then new water molecules were added using ARP/wARP<sup>6</sup> in the final cycles. Statistics of the refinement and the final model are listed in Table S2.

**Table S2. Refinement statistics**

Resolution range (highest shell) ( $\text{\AA}$ )	38.95-1.74 (1.79-1.74)
Completeness (%)	95.4
Free R-factor test set ( $\text{\AA}$ %)	3247, 5.0
R-factor (R-free)	0.1978 (0.2312)
Mean B-factor ( $\text{\AA}^2$ )	32.4
R.m.s.d. bonds ( $\text{\AA}$ )	0.010
R.m.s.d. angles (degrees)	1.19
Contents of model ( $\text{\AA}$ atoms, mean B-factors ( $\text{\AA}^2$ ))	
Molecule A (aa $\text{\AA}$ : 224-276,278-510)	2337, 25.21
Imatinib A	37, 19.28
GNF-2 A	27, 28.99
Molecule B (aa $\text{\AA}$ : 225-274,278-510)	2299, 38.62
Imatinib B	37, 26.92
GNF-2 B	27, 60.45
Solvent (waters; chloride)	429, 37.77; 1, 31.53
Ramachandran outliers	Lys245, Arg362 (0.72%)

### Structure analysis:

Density for GNF-2 in molecule A is stronger than for molecule B (Figure S2). The binding site on molecule B is only partially occupied, so the discussion of the structure in the main text is focused on molecule A. For GNF-2 bound to molecule A, the density is also weak for the amide substituent of the benzamide due to flexibility in the crystals. Therefore, the position of this group is not well defined. Distances between GNF-2 and Abl kinase in the binding site are listed for both molecules in Table S3.

**Table S3. Distances between protein and ligand less than or equal to 3.8  $\text{\AA}$ . Distances greater than 3.8  $\text{\AA}$  are not listed.**

Ligand atom	Protein atom	Distance Mol A	Distance Mol B
F1	Phe 493 CE1	3.62	3.50
	Leu 341 CA	3.77	3.72
	Leu 341 CD1	3.78	
	Ala 344 CB	3.44	3.64
	Leu 429 CD1	3.68	3.78
F3	Val 468 CG1	3.71	3.55
	Leu 429 CD1	3.09	3.19
F4	Leu 340 C	2.94	3.00
	Leu 341 N	3.08	3.17
	Leu 341 CA	3.35	3.44
	Leu 340 O	2.94	2.98
	Leu 340 CA	3.78	3.79
	Leu 340 CB	3.44	3.39
	Ile 432 CG2	3.50	3.49
O5	Val 468 CG2	3.76	3.74
	Ile 502 CD1	3.60	3.76
C6	Ile 502 CD1	3.75	
C7	Ala 337 O	3.75	3.77
	Leu 340 CB		3.66
	Ile 502 CD1	3.46	
C9	Leu 340 CD1	3.66	3.40
	Ala 337 CB	3.74	
C12	Pro 465 CD	3.68	3.70
	Ala 433 CB	3.63	3.66
	Cys 464 CA	3.80	
N16	Ala 433 O		3.77
N19	Val 506 CG1		3.77
	Leu 340 CD1	3.70	
	Ala 337 CB	3.66	
C20	Tyr 435 OH	3.50	3.73
C24	Glu 462 O		3.62
C27	Leu 510 CD1	3.77	
C29	Leu 510 CD1	3.72	
C32	Glu 462 OE1		3.59
C34	Glu 462 O	3.54	3.64
O37	Leu 510 CD1	3.16	3.65
N16	244/6 OW0	2.90	2.75
244/6 OW0	Ala 433 O	2.88	2.87
	Glu 462 O	2.85	2.87
N22	/44 OW0	3.09	
/44 OW0	Tyr 435 OH	2.90	
	/136 OW0	2.68	
N38	/136 OW0	2.97	

## Synthetic Chemistry

**GNF-2** [3-(6)-(4-Trifluoromethoxy-phenylamino)-pyrimidin-4-yl]-benzamide]: A mixture of (4-chloro-6-(4-trifluoromethoxy-phenylamino)-pyrimidine (200 mg, 0.69 mmol), 3-carbamoylphenylboronic acid (115 mg, 0.69 mmol), palladium tetrakis(triphenylphosphine) (40 mg, 0.034 mmol) and sodium carbonate (292 mg, 2.76 mmol) in acetonitrile/water (1:1, v/v, 10 mL) was heated to 90°C under an argon atmosphere. After refluxed for 8 h, the reaction mixture was cooled to room temperature and concentrated *in vacuo*. The resulting crude product was purified by flash column chromatography (SiO<sub>2</sub>, ethyl acetate/hexanes (v/v) = 1/1) to yield GNF-2 (206 mg, 80 %) as white solid. <sup>1</sup>H NMR (400 MHz, DMSO-d<sub>6</sub>): 8.79 (s, 1H), 8.53 (s, 1H), 8.23 (d, *J* = 8.5Hz, 1H), 7.96 (d, *J* = 5.1Hz, 1H), 7.85 (d, *J* = 6.9Hz, 2H), 7.75 (t, *J* = 7.9Hz, 1H), 7.48 (s, 2H), 7.36 (d, *J* = 8.2Hz, 2H), 7.33 (s, 1H). MS: *m/z* 375.1 (M+1).

**GNF-5** N-(2-hydroxyethyl)-3-(6-(4-(trifluoromethoxy)phenylamino)pyrimidin-4-yl)benzamide: 3-[6-(4-Trifluoromethoxy-phenylamino)-pyrimidin-4-yl]-benzoic acid: Synthesized analogously to GNF-2 by using 3-carboxyphenylboronic acid: A mixture of 6-chloro-N-(4-(trifluoromethoxy)phenyl)pyrimidin-4-amine (200 mg, 0.69 mmol), 3-carboxyphenylboronic acid (115 mg, 0.69 mmol), Pd(PPh<sub>3</sub>)<sub>4</sub> (40 mg, 0.034 mmol), and sodium carbonate (292 mg, 2.76 mmol) in acetonitrile/water (v/v = 1/1, 10 mL) was heated to 90°C under an argon atmosphere. After refluxed for 8 h, the hot reaction mixture was filtered. The filtrate was cooled to room temperature, treated with 6 N HCl (pH is around 4) to afford 3-(6-(4-(trifluoromethoxy)phenylamino)pyrimidin-4-yl)benzoic acid as a pale yellow precipitate, which was collected and washed with water: <sup>1</sup>H NMR (600 MHz, DMSO-*d*<sub>6</sub>) 11.28 (s, br, 1H), 8.87 (s, 1H), 8.51 (d, *J* = 1.2 Hz, 1H), 8.21 (dd, *J* = 1.2, 8.4 Hz, 1H), 8.13 (d, *J* = 7.2 Hz, 1H), 7.88 (d, *J* = 9.0 Hz, 2H), 7.73 (t, *J* = 7.8 Hz, 1H), 7.54 (s, 1H), 7.40 (d, *J* = 9.0 Hz, 2H); MS: *m/z* 376 (M+1).

To a solution of 3-[6-(4-trifluoromethoxy-phenylamino)-pyrimidin-4-yl]-benzoic acid (81 mg, 0.22 mmol), ethanolamine (16 mg, 0.26 mmol), and diisopropylethylamine (84 mg, 0.65 mmol) in dimethylformamide (0.5 mL) was added 2-(1H-7-azabenzotriazol-1-yl)-1,1,3,3-tetramethyluranium "HATU" (99 mg, 0.26 mmol) at room temperature. The reaction mixture was stirred for 4 h at room temperature and directly purified by flash column chromatography (SiO<sub>2</sub>, CH<sub>2</sub>Cl<sub>2</sub>/MeOH (v/v) = 20/1) to afford GNF-5 (80 mg, 89%) as white solid. <sup>1</sup>H NMR (400MHz, CDCl<sub>3</sub>), 9.95 (s, 1H), 8.78 (s, 1H), 8.64 (t, *J* = 5.6Hz, 1H), 8.53 (s, 1H), 8.19 (d, *J* = 8.0Hz, 1H), 7.99 (d, *J* = 8.0Hz, 1H), 7.86 (d, *J* = 8.4Hz, 2H), 7.63 (t, *J* = 7.6Hz, 1H), 7.36 (d, *J* = 8.4Hz, 2H), 7.34 (s, 1H), 4.76 (t, *J* = 5.6Hz, 1H), 3.54 (dd, *J* = 6.0Hz, 2H), 3.37 (dd, *J* = 6.0Hz, 2H); MS *m/z* 419.2 (M+1).

**Compound 6.** N4-(2-morpholinoethyl)-N2-(4-(trifluoromethoxy)phenyl)pyrimidine-2,4-diamine: To a solution of 2,4-dichloropyrimidine (300 mg, 2.0mmol) in isopropanol (10 mL) were added 2-morpholinoethanamine (130 mg, 1.0 mmol) and DIEA (350 μL, 2.0 mmol). The reaction mixture was stirred at room temperature for 16 h and concentrated. The resulting crude product was purified by flash column chromatography (SiO<sub>2</sub>, ethyl acetate/hexanes (v/v) = 1/1) to afford 2-chloro-N-(2-morpholinoethyl) pyrimidin-4-amine (205 mg, 85%) as a pale yellow solid. To a solution of 2-chloro-N-(2-

morpholinoethyl)pyrimidin-4-amine (30 mg, 0.124 mmol) in 1-butanol (2 mL) were added 4-(trifluoromethoxy)benzenamine (24 mg, 0.135 mmol) and 6 N HCl (22.5  $\mu$ L). The reaction mixture was stirred at 90 °C for 4 h and concentrated. The resulting crude product was purified by preparative LC/MS to yield the desired compound (31 mg, 65%) as a white solid.

**Compound 7.** Synthesized using the same procedure as compound 6 using 2,4-dichlorotriazine as the starting material.

**Compound 8.** Synthesized using the same procedure as compound 6 using 2,4-dichloro-5-methylpyrimidine as the starting material

Compound	Chemical formula	M.W.	<sup>1</sup> H NMR (400 MHz)	Mass spectrum <i>m/z</i> (M+1)
GNF-1	C <sub>17</sub> H <sub>20</sub> F <sub>3</sub> N <sub>5</sub> O <sub>2</sub>	383.37	CDCl <sub>3</sub> , 8.21 (s, 1H), 7.76 (s, 1H), 7.34 (d, <i>J</i> =8.2Hz, 2H), 7.20 (d, <i>J</i> =8.4Hz, 2H), 5.89 (s, 1H), 3.69 (t, <i>J</i> =4.7Hz, 4H), 2.27(d, <i>J</i> =4.3Hz, 2H), 2.58 (t, <i>J</i> =5.2Hz, 2H), 2.45 (t, <i>J</i> =5.3Hz, 4H)	384.20
GNF-2	C <sub>18</sub> H <sub>13</sub> F <sub>3</sub> N <sub>4</sub> O <sub>2</sub>	374.32	DMSO- <i>d</i> <sub>6</sub> , 8.79 (s, 1H), 8.53 (s, 1H), 8.23 (d, <i>J</i> =8.5Hz, 1H), 7.96 (d, <i>J</i> =5.1Hz, 1H), 7.85 (d, <i>J</i> =6.9Hz, 2H), 7.75 (t, <i>J</i> =7.9Hz, 1H), 7.48 (s, 2H), 7.36 (d, <i>J</i> =8.2Hz, 2H), 7.33 (s, 1H)	375.10
GNF-5 <sup>a</sup>	C <sub>20</sub> H <sub>17</sub> F <sub>3</sub> N <sub>4</sub> O <sub>3</sub>	418.37	CDCl <sub>3</sub> , 9.95 (s, 1H), 8.78 (s, 1H), 8.64 (t, <i>J</i> =5.6Hz, 1H), 8.53 (s, 1H), 8.19 (d, <i>J</i> =8.0Hz, 1H), 7.99 (d, <i>J</i> =8.0Hz, 1H), 7.86 (d, <i>J</i> =8.4Hz, 2H), 7.63 (t, <i>J</i> =7.6Hz, 1H), 7.36 (d, <i>J</i> =8.4Hz, 2H), 7.34 (s, 1H), 4.76 (t, <i>J</i> =5.6Hz, 1H), 3.54 (dd, <i>J</i> =6.0Hz, 2H), 3.37 (dd, <i>J</i> =6.0Hz, 2H)	419.20
6	C <sub>17</sub> H <sub>20</sub> F <sub>3</sub> N <sub>5</sub> O <sub>2</sub>	383.37	N/A	384.10
7				
8	C <sub>18</sub> H <sub>22</sub> F <sub>3</sub> N <sub>5</sub> O <sub>2</sub>	397.39	N/A	398.10

## SUPPLEMENTRAY FIGURE LEGENDS

**Supplementary Figure 1. Difference electron density and crystal structure for GNF-2 bound to Abl kinase.** The Fo-Fc Fourier map, calculated before fitting the ligand to the model, is contoured at 3.0  $\sigma$  for the two molecules of GNF-2 in the asymmetric unit. Density for molecule **a** is shown on the left and that for molecule **b** on the right. **c**, Stereo view of the GNF-2-Abl interactions: Abl kinase is indicated in green (helices indicated with transparent cylinders) with the bent part of the I-helix in yellow, GNF-2 resistance mutations in pink, and GNF-2 carbons in cyan. H-bonding and other polar interactions are indicated by dotted red lines. A water molecule forms a hydrogen bond bridge between the aniline NH and the main chain carbonyls of A433 and E462 in both the fully and partially occupied myristate binding sites in the crystal. Residues contacting GNF-2 at the base of the pocket are L341 and A344 from E, I432 from F, V468 from H, F493 from I and I502 from I'. The surface in the central part of the pocket is formed by A337 from E, C464 and P465 from the start of H, A433 from F, and V506 from I'. There are fewer interactions at the mouth of the pocket (Y435 from  $\alpha$ F, E462 from the loop before  $\alpha$ H and L510 at the end of I'), which is reflected in the weak electron density and hence flexibility of the benzamide part of GNF-2. Mutations, C464Y, P465S, and V506L presumably confer direct steric hindrance to the binding of GNF-2, while F497L and E505K are in the second shell of residues forming the binding site, and are likely to have an indirect unfavorable steric effect. The overall structure of the Abl kinase domain complexed to GNF-2 is similar to that of the myristate complex, except for the positions of residues between F497 and S501 which are shifted by up to 4 Å. This is due to crystal contacts between this part of the structure and a neighboring molecule in the crystal. GNF-2 does not affect the myristate binding site but the SH2-docking surface is altered to prevent clash between its helix  $\alpha$ A and the ligand. There is also a very small rotation of the N-terminal lobe of the kinase with respect to the C-terminal lobe, but this may also be due to slight changes in crystal packing due to the replacement of the myristoylated peptide. There is very little difference between the relative orientations of these lobes when comparing the Abl/imatinib complex<sup>7</sup> with the Abl/imatinib/myristate complex<sup>1,8</sup>.

**Supplementary Figure 2. Structure-activity relationships (SAR) for GNF-2 & 5.** **a**, Structures of GNF-2 and GNF-5 highlighting features important for Bcr-Abl inhibitory activity. Structure-activity relationships revealed a strict requirement for the para-trifluoromethoxyaniline substituent, the aniline-NH, and the 4,6-disubstituted pyrimidine. The pyrimidine C4-position tolerated a variety of substituents, but optimal cellular potency as a Bcr-Abl inhibitor was achieved with either meta- or para-substituted phenyls, such as meta-carboxamido (3-CONH<sub>2</sub> (GNF-2), 3-CONH(CH<sub>2</sub>)<sub>2</sub>OH (GNF-5), sulfones (SO<sub>2</sub>CH<sub>3</sub>), and sulfonamides (SO<sub>2</sub>NHR). Further structure-activity relationships studies indicated that the bioactive conformation of GNF-2 involves a trans-orientation between the 4-trifluoromethoxyaniline and the pyrimidine motif such that the compound assumes an extended conformation. **b**, GNF-5 against a range of clinically observed imatinib-resistant Bcr-Abl mutations.

**Supplementary Figure 3. GNF-2 resistance mutation screen.** **a**, Frequency of various GNF-2 resistance mutations recovered from a cell-based mutagenesis screen (blue) and a random mutagenesis screen (red). Among those mutations, P465S and E505K account for 64% of total mutations recovered in the presence of 5 or 10  $\mu\text{M}$  of GNF-2 in the cell based screen, while 53% of the mutations identified from the random mutagenesis screen with 2.8  $\mu\text{M}$  GNF-2 correspond to C464Y and E505K. **b**, Overview of the Abl structure (PDB ID 1OPK<sup>1</sup>) with representative GNF-2 resistance mutations indicated by red balls, the size of spheres is proportional to the frequency with which that mutation was recovered in the screen.

**Supplementary Figure 4. Characterization of GNF-2 resistance mutations** **a**, The ability of GNF-2 or imatinib (10  $\mu\text{M}$ ) to inhibit cellular Bcr-Abl kinase activity in wild-type and mutant expressing cells was tested by monitoring phospho-Bcr-Abl and phospho-STAT5 following treatment of cells with inhibitor for 2 hours. **b**, Chemical structures of GNF-2, GNF-5, and GNF-2-Affigel-10. **c**, Ability of wild-type and mutant Bcr-Abl to bind to GNF-2 affinity support. Western blot with the anti-Abl antibody K-12 detects the amount of wild type or mutant Bcr-Abl from cell lysates retained on the GNF-2 affinity resin in the presence or absence of 50  $\mu\text{M}$  competitive GNF-2.

**Supplementary Figure 5. NMR-detected titration of GNF-2 to Abl complexes.** The upfield parts of NMR spectra are shown (left) which include an Abl methyl group near the myristate pocket. Chemical shift changes of this methyl group are followed as GNF-2 is added at concentrations up to its solubility limit of 30  $\mu\text{M}$ . The chemical shift changes plotted versus GNF-2 concentration directly yield the dissociation constant (right). **a**, 15  $\mu\text{M}$  wildtype Abl(229-500), **b**, 15  $\mu\text{M}$  T315I Abl(229-500), **c**, 10  $\mu\text{M}$  wildtype Abl(229-515). Although binding of GNF-2 to wt Abl(229-515) shows signs of slow to intermediate exchange for some resonances, the  $K_D$  could be unambiguously determined:  $0.5 \pm 0.1 \mu\text{M}$  for GNF-2 binding to the imatinib/Abl complex using the full-length catalytic domain (residues 229-515; Abl 1a numbering – panel c), and  $7.4 \pm 1.5 \mu\text{M}$  using the imatinib/Abl complex with a C-terminal truncated form of Abl (residues 229-500) not including helix I (panel a) and  $13.5 \pm 1.8 \mu\text{M}$  using the T315I mutant of a C-terminal truncated form of Abl (residues 229-500) not including helix I (panel b). The lower affinity to the (229-500) construct is probably due to the lack of helix I, which lines the myristate pocket and is involved in interactions with GNF-2.

**Supplementary Figure 6. Inhibition of GNF-5 and combination with nilotinib.** **a**, Inhibition of STAT5 phosphorylation in T315I Bcr-Abl Ba/F3 cells in the presence of nilotinib (10  $\mu\text{M}$ ) or GNF-5 (1  $\mu\text{M}$ ) alone or in combination. Inhibition of STAT5 phosphorylation is reversed upon addition of interleukin-3 (IL-3). **b**, Nilotinib and GNF-5 exhibited cooperativity for inhibition of wild-type Bcr-Abl transformed BaF3 cells with a calculated combination index of 0.61. An enlargement of the region where cooperativity between the agents is apparent is shown in the right corner. The combination curve (red) contains twice the total drug concentration of the single agent curves due to the presence of both drugs. **c**, Nilotinib's anti-proliferative  $\text{EC}_{50}$  in the presence of 1 to 10  $\mu\text{M}$  GNF-5 on Ba/F3 cells expressing T315I Bcr-Abl. **d**, Effects of GNF-5 in combination with varying concentrations of nilotinib (0.6-20  $\mu\text{M}$ ) on the

proliferation of T315I Bcr-Abl and T315I/E505K Bcr-Abl expressing Ba/F3 cells **e**, Effects of GNF-5, nilotinib, and varying concentrations of GNF-5 in combination with nilotinib (0.3-10  $\mu\text{M}$ ) on the proliferation of T315I Bcr-Abl Ba/F3 cells. Note that the combination curve (red, as well in **f**) shows the total combined concentration of both drugs and the actual dosage of each drug was only half that present in the corresponding single agent curves. Plots **e** and **f** represent the same data as shown in Figure 4a and **c** respectively but are replotted here so the single agent and combination curves can be compared on the basis of equal amounts of total drug. **f**, Percent inhibition of T315I Abl kinase by nilotinib, GNF-5, or the combination.

**Supplementary Figure 7. Combinations of GNF-5 and nilotinib synergize to inhibit p190 Bcr-Abl transformed BaF3 cells.** **a**, Growth inhibition curves with the indicated combinations of GNF-5 and nilotinib. The combination curve (red) contains twice the total drug concentration of the single agent curves due to the presence of both drugs. **b**, Table of calculated combination indices.

**Supplementary Figure 8. Mass spectra of the Abl proteins: wild-type, E505K, and T315I.** The raw  $m/z$  data are shown on the left, and the transformed, mass only spectra shown on the right. The measured and theoretical molecular weights of the unmodified form of each protein are indicated. In the transformed mass spectra, peaks corresponding to each phosphorylation are indicated.

**Supplementary Figure 9. GNF-5 inhibits Abl kinase in a non-ATP competitive fashion** **a**, Abl kinase activity was measured in a PEP-LDH coupled assay at different ATP concentrations, using formation of NAD as the indicator of reaction. Enzyme activity was measured in the presence of 0, 0.2, 0.8, and 1.6  $\mu\text{M}$  GNF-5 with increasing concentrations of ATP. **b**, As in **a** with imatinib instead of GNF-5. Each data point is the average of three independent experiments. Data are plotted in double-reciprocal form to determine  $K_m$  and  $V_{max}$  with ATP concentration ranging from 2.5 to 160  $\mu\text{M}$ . For imatinib (Gleevec), the value is constant at  $4.18 \pm 0.5$ ,  $4.46 \pm 0.5$ , and  $4.25 \pm 0.6 \text{ mU min}^{-1}$  in the presence of 0, 0.2, and 0.8  $\mu\text{M}$  imatinib concentrations, respectively. This is as expected for an ATP-competitive inhibitor. In contrast,  $V_{max}$  decreases with increasing concentrations of GNF-5, and these effects are clearly seen in the double-reciprocal plot. For GNF-5, the value of  $V_{max}$  decreases from  $4.18 \pm 0.5$  in the absence of GNF-5 to  $2.43 \pm 0.2$  and  $2.2 \pm 0.2 \text{ mU min}^{-1}$  in the presence of 0.2 and 0.8  $\mu\text{M}$  GNF-5, respectively. These kinase assay results demonstrate that the mechanism of Abl inhibition by GNF-5 is non-competitive with respect to ATP and that no additional co-factors are needed to observe inhibition *in vitro*. **c**, Fluorescence polarization titration of GNF-2 with wild-type Abl using GNF-2-FITC. Chemical structure of GNF-2-FITC modified compound. **d**, Fluorescence polarization titration of GNF-2 with wild-type Abl using GNF-2-FITC probe yields and  $\text{EC}_{50}$  of 169 nM.

**Supplementary Figure 10. Enzymatic inhibition of wild-type Abl kinase by combination treatments.** **a**, Inhibition of wild-type Abl kinase activity by nilotinib in the presence of increasing concentrations of GNF-5. **b**,  $\text{IC}_{50}$  values for inhibition of wild-type Abl by nilotinib with increasing concentrations of GNF-5. Error bars are s.e.m.

**Supplementary Figure 11. GNF-5 pharmacokinetic parameters in mice.** Following an oral dose of 20 mg/kg to Balb/C mice, GNF-5 appeared rapidly in the circulation to attain a maximum concentration of  $4.4 \pm 1.3 \mu\text{M}$  at 0.5 h, decreasing to  $0.63 \pm 0.12 \mu\text{M}$  after 7 hours, with a terminal half-life of 2.3 hours; oral bioavailability was  $44.8 \pm 7.5\%$ . In SCID mice, as used for efficacy studies in the xenograft model, the pharmacokinetic profile in plasma was similar to that observed in normal mice. **a**, GNF-5 plasma concentration (nanomolar) versus time (hours) following intravenous and oral doses of 5 mg/kg and 20 mg/kg, respectively. **b**, Pharmacokinetic parameters: AUC = area under the curve (measure of exposure),  $C_{\text{max}}$  = maximum plasma concentration,  $T_{\text{max}}$  = time of maximum plasma concentration,  $C_{\text{last}}$  = concentration at last measured time point,  $T_{1/2}$  = time required for plasma concentration to reach half of the highest concentration,  $V_{\text{ss}}$  = volume of distribution, F = percentage oral bioavailability.

**Supplementary Figure 12. *In vivo* efficacy studies with GNF-5 on Bcr-Abl dependent proliferation in xenograft model.** Quantification of tumor/control of whole body luminescence of wild-type Bcr-Abl and luciferase expressing Ba/F3 cells on days five and seven after treatment with vehicle, GNF-5 50 mg/kg and 100 mg/kg b.i.d.

**Supplementary Figure 13. GNF-5 efficacy correlates with inhibition of Bcr-Abl-mediated STAT5 phosphorylation.** Phospho-STAT5 (blue curves) was monitored by FACS at various time-points and doses (indicated on left). Each box corresponds to an individual animal.

**Supplementary Figure 14. GNF-5 treatment normalizes blood counts and spleen size of Bcr-Abl BMT mice.** Bone marrow cells from donor mice pretreated with 5-fluorouracil (5-FU) were transduced with a wild-type Bcr-Abl retroviral vector and transplanted into irradiated recipient mice. Seven days after transplantation, a dose regimen consisting of 50 mg/kg GNF-5 twice daily or vehicle was administered during seven days. Peripheral blood cell counts measured on the last day of treatment were high, with 95% neutrophils or blast cells, in the vehicle treated mice, consistent with development of CML-like disease. In contrast, GNF-5 treated mice showed normal blood cell counts. The spleen size from the vehicle group was increased 3- to 4-fold compared to those of normal mice (normal spleen weight: 80-90 mg), while GNF-5 treated mice had normal spleen weights. Error bars are s.e.m.

**Supplementary Figure 15. Differential scanning calorimetry (DSC).** **a**. Samples consisting of 1mg/ml of wt Abl (46-531) mixed with DMSO or imatinib (STI571) at 10  $\mu\text{M}$  final concentration or GNF-2 at 20  $\mu\text{M}$  final concentration in 20mM Tris pH 8.0, 5% glycerol, 1mM TCEP buffer were subjected to DSC. The results indicate that both STI-571 and GNF-2 bind to Abl (46-531). **b**. Samples consisting of 1mg/ml of wt Abl (46-531) mixed with DMSO, GNF-2, or Me-GNF-2 (inactive analog of GNF-2) at 20  $\mu\text{M}$  final concentration, or 1mg/ml of wt Abl (46-531) pre-incubated with imatinib at 10  $\mu\text{M}$  for 30 min and to which GNF-2 was added at 20  $\mu\text{M}$  final concentration were subjected to DSC. **c**. The increase in melting temperature observed in the presence of both compounds suggests strongly that binding of both compounds causes additional stabilization of the kinase relative to the kinase bound to only one of the compounds.

- <sup>1</sup> Nagar, B. et al., Structural basis for the autoinhibition of c-Abl tyrosine kinase. *Cell* **112** (6), 859 (2003).
- <sup>2</sup> Kroemer, M., Dreyer, M. K., and Wendt, K. U., APRV - a program for automated data processing, refinement and visualization. *Acta Crystallogr D Biol Crystallogr* **60** (Pt 9), 1679 (2004).
- <sup>3</sup> Kabsch, W., Automatic processing of rotation diffraction data from crystals of initially unknown symmetry and cell constants. *Journal of Applied Crystallography* **26** (6), 795 (1993).
- <sup>4</sup> Murshudov, G. N., Vagin, A. A., and Dodson, E. J., Refinement of macromolecular structures by the maximum-likelihood method. *Acta Crystallogr D Biol Crystallogr* **53** (Pt 3), 240 (1997).
- <sup>5</sup> Emsley, P. and Cowtan, K., Coot: model-building tools for molecular graphics. *Acta Crystallogr D Biol Crystallogr* **60** (Pt 12 Pt 1), 2126 (2004).
- <sup>6</sup> Perrakis, A., Sixma, T. K., Wilson, K. S., and Lamzin, V. S., wARP: improvement and extension of crystallographic phases by weighted averaging of multiple-refined dummy atomic models. *Acta Crystallogr D Biol Crystallogr* **53** (Pt 4), 448 (1997).
- <sup>7</sup> Nagar, B. et al., Crystal structures of the kinase domain of c-Abl in complex with the small molecule inhibitors PD173955 and imatinib (STI-571). *Cancer Res* **62** (15), 4236 (2002).
- <sup>8</sup> Hantschel, O. et al., A myristoyl/phosphotyrosine switch regulates c-Abl. *Cell* **112** (6), 845 (2003).